Supplementary material

Morphology-Enhanced Piezoelectric Performance of SnS Nanobelts for Acetaminophen Degradation

Shuhui Liu,[a] Huayang Zhang,[a] Yantao Wang,[a] Hongqi Sun,[b] Shaobin Wang,[a*] and Wenjie Tian[a*]

[a] School of Chemical Engineering, The University of Adelaide, Adelaide, SA 5005, Australia

[b] School of Molecular Sciences, The University of Western Australia, Perth, WA 6009 Australia

* Corresponding authors.

Email: shaobin.wang@adelaide.edu.au; wenjie.tian@adelaide.edu.au

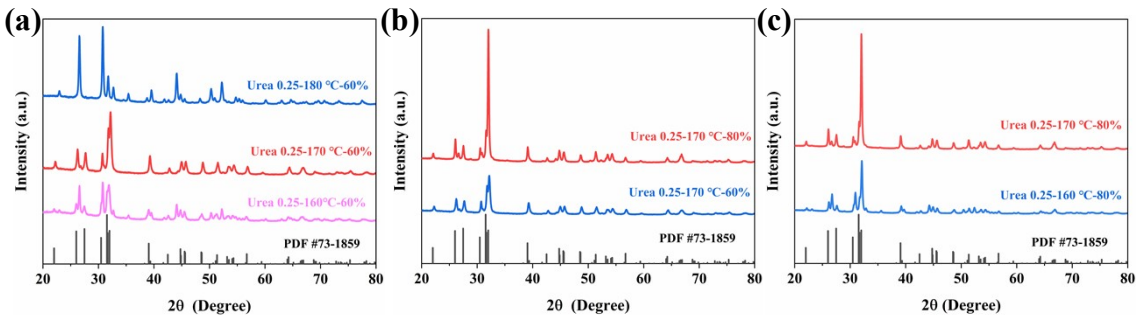

Fig. S1 XRD patterns of SnS synthesized under different conditions with the addition of 0.25 M urea. (a) different temperature with 60% volume, (b) different volume, (c) different temperature with 80% volume.

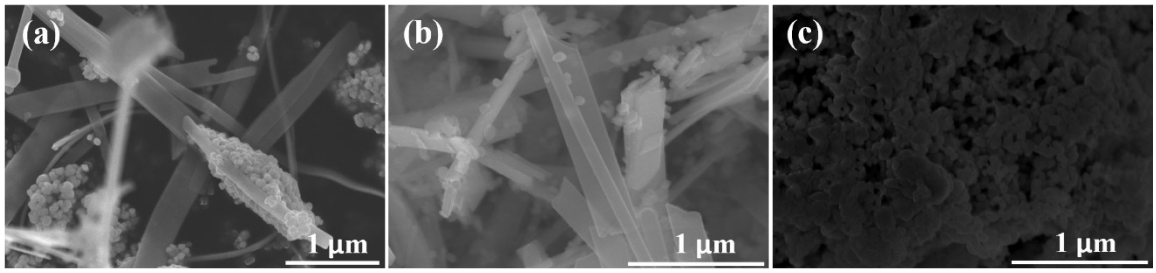

Fig. S2 SEM images of SnS-0.25 samples with different synthesized temperature (0.25 M urea, 80% volume), (a) 160 °C, (b) 170 °C, (c) 180 °C.

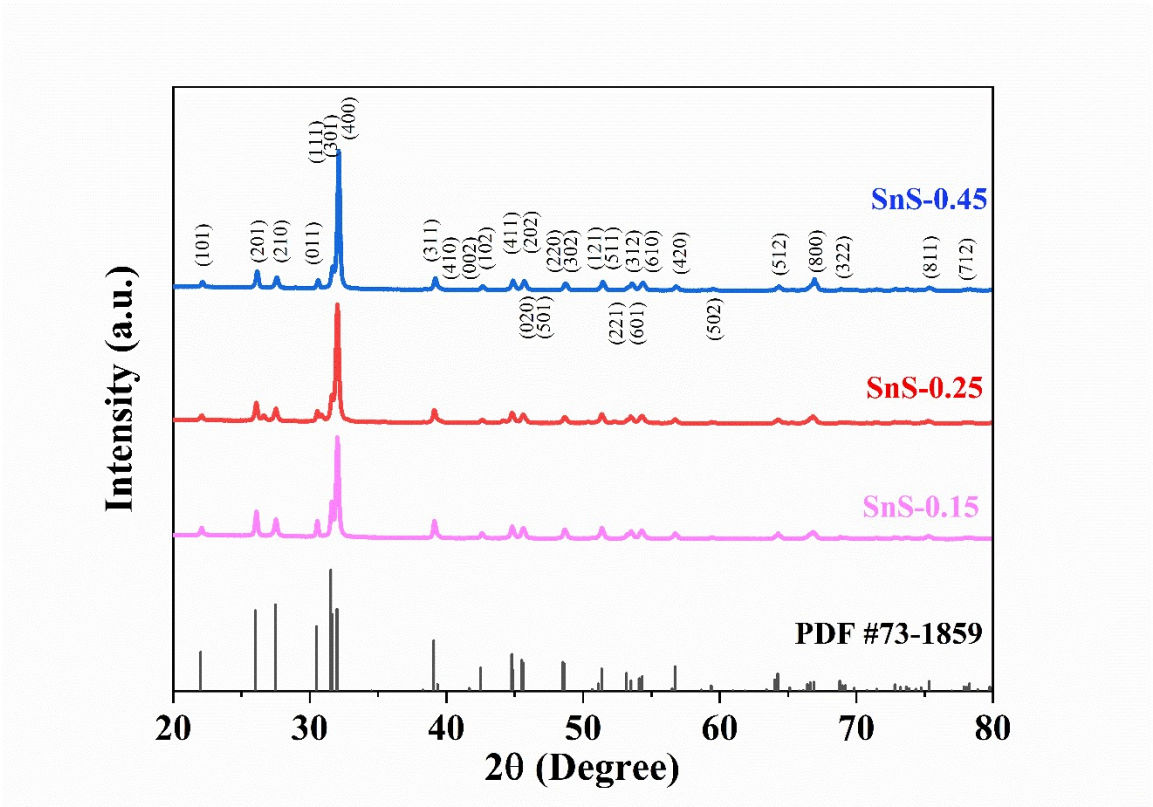

Fig. S3 XRD patterns of SnS nanobelts synthesized at 170 °C, 80% reaction solution volume and different contents of urea.

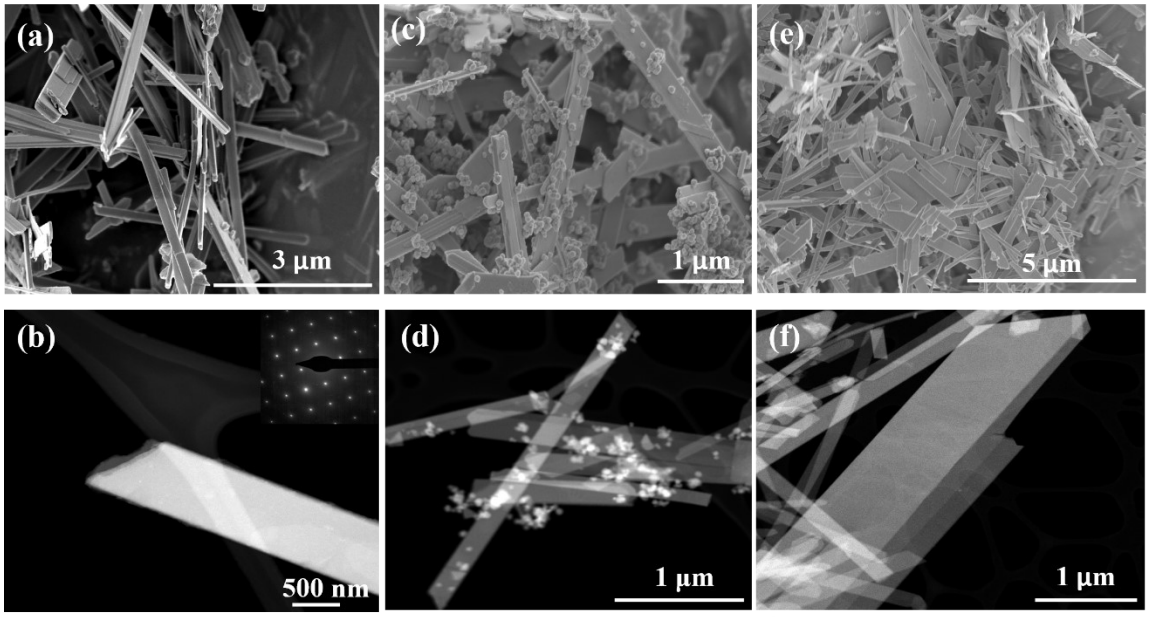

Fig. S4 SEM and TEM images of SnS synthesized at 170 °C, 80% reaction solution volume ratio and varied urea amounts (0.15-0.45 M). (a, b) SnS-0.15. (c, d) SnS-0.25. (e, f) SnS-0.45.

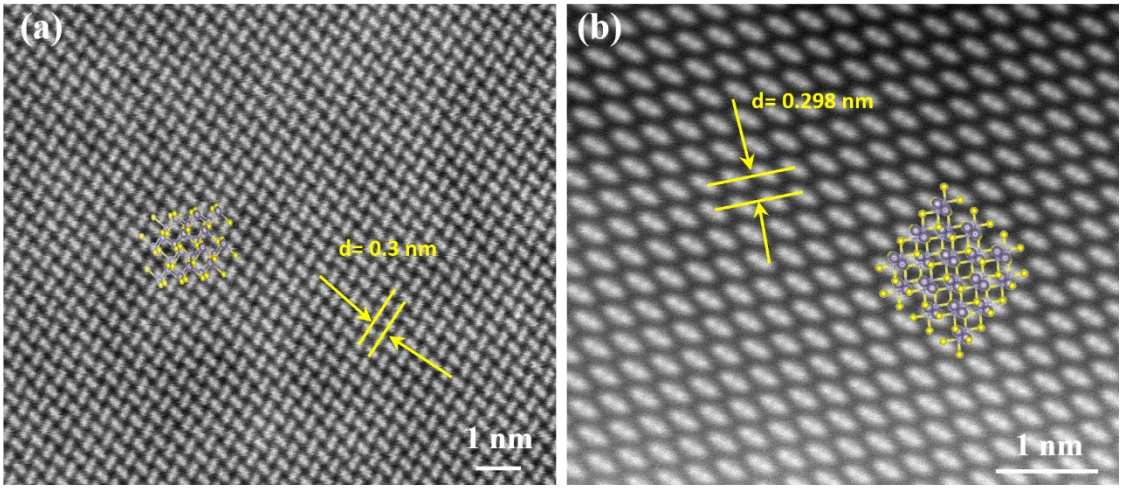

Fig. S5 High-angle annular dark-field (HAADF)-STEM images of SnS-0.15, and the crystallographic directions along (a) [-101] band axes, (b) [001] band axes.

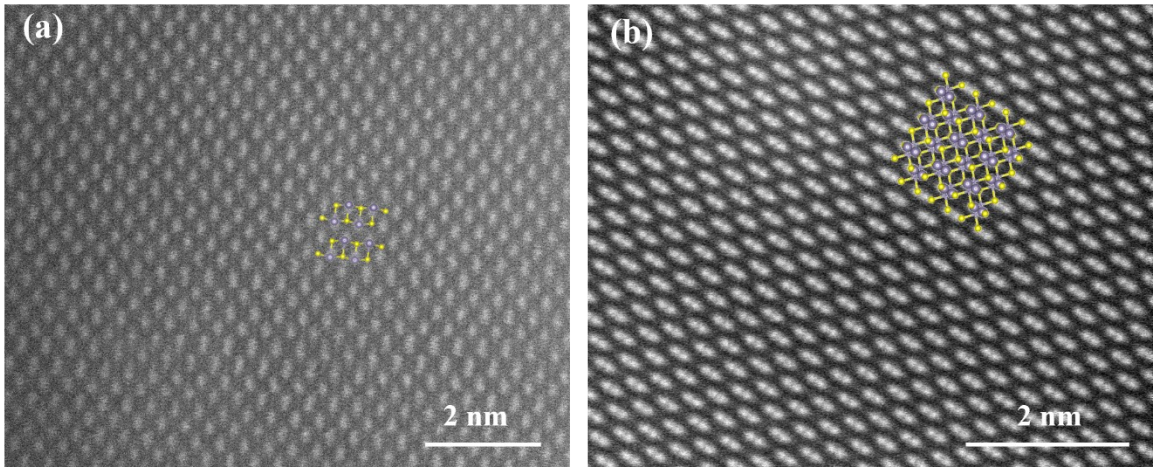

Fig. S6 High-resolution HAADF-STEM images of (a) SnS-0.25, and (b) SnS-0.45.

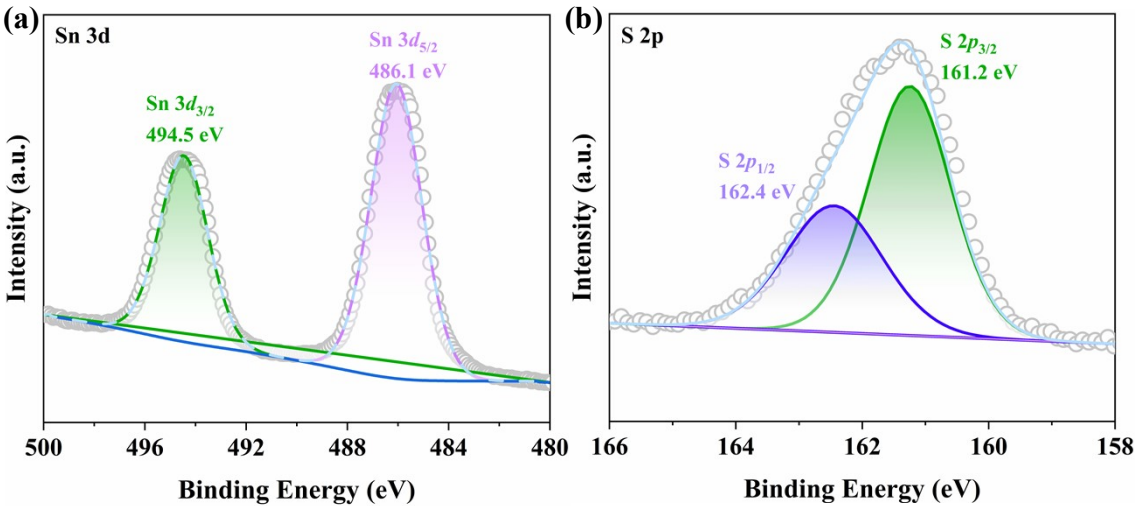

Fig. S7 XPS spectra of SnS-0.15, (a) Sn 3d, (b) S 2p.

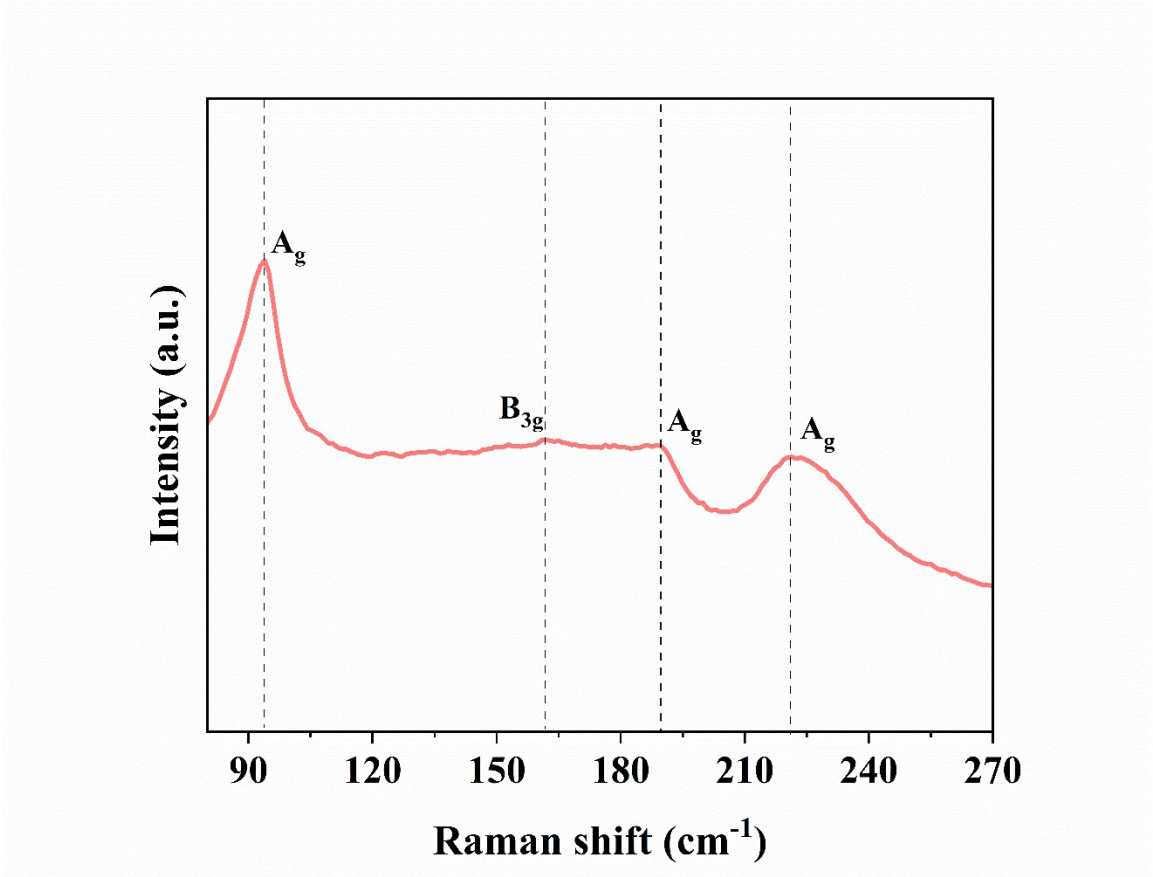

Fig. S8 Raman spectrum of SnS-0.15.

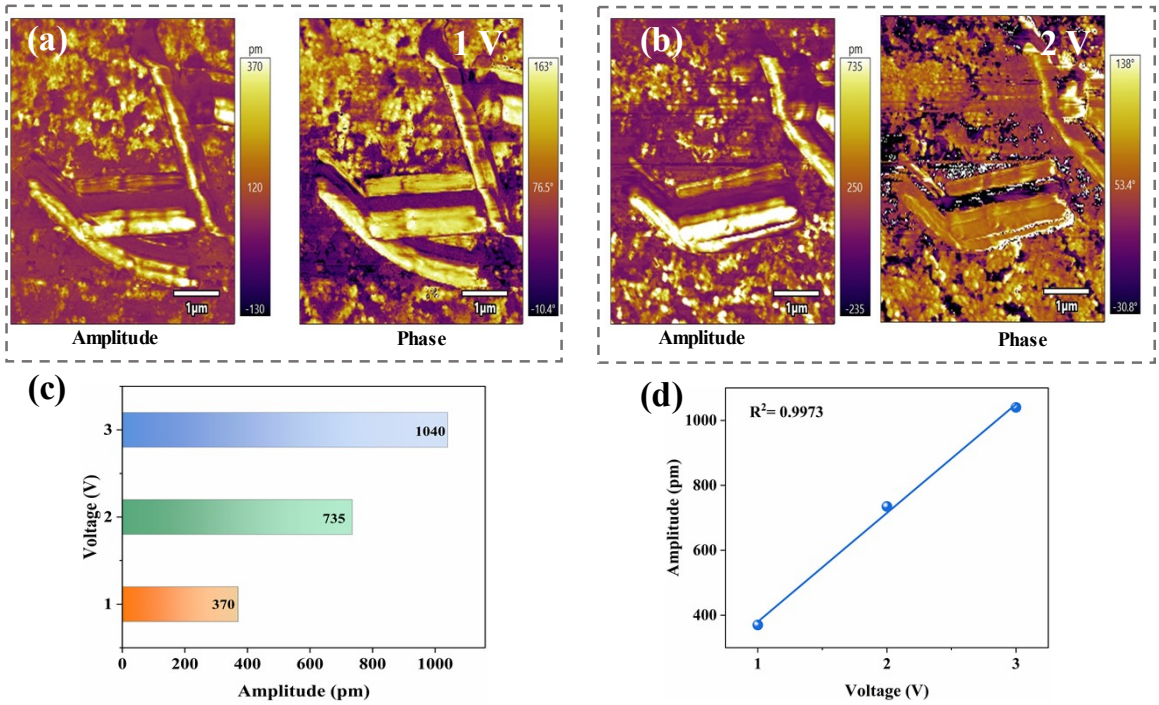

Fig. S9 Piezoelectric response amplitude profiles and phase images of SnS-0.15 at different driving forces: (a) 1 V, (b) 2 V, (c, d) piezoresponse amplitude as a function of the applied driving voltages.

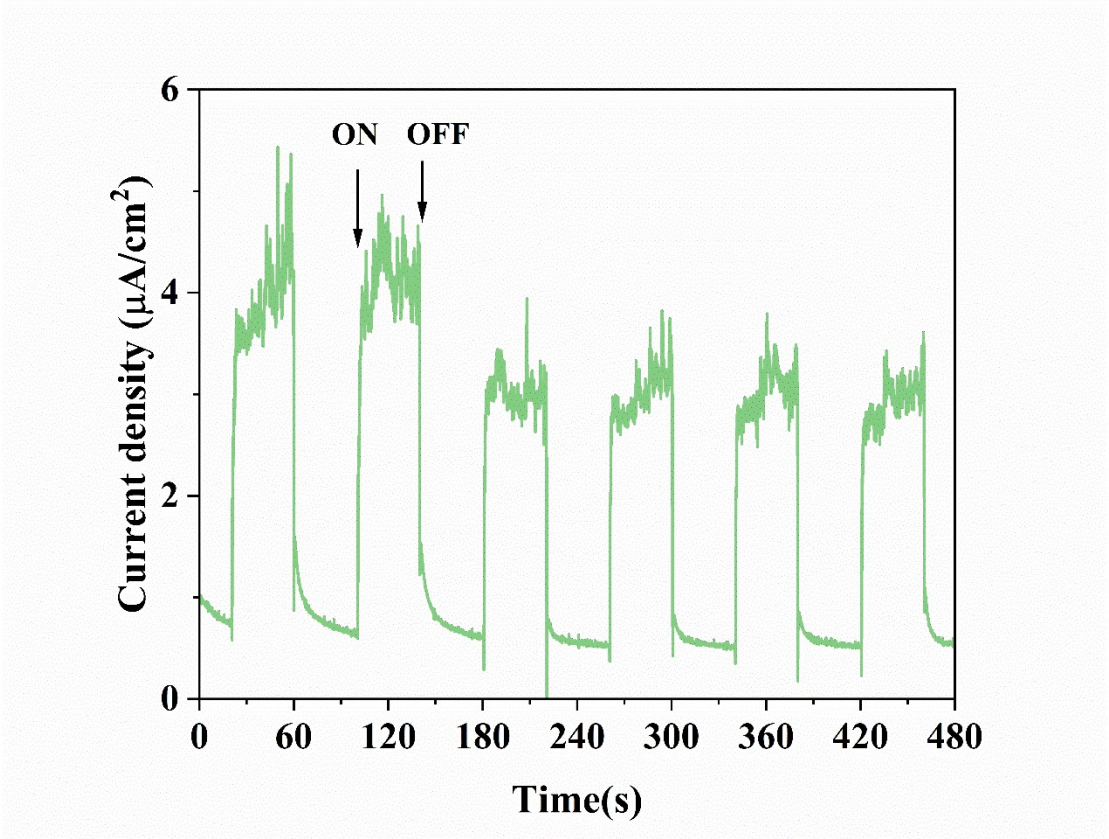

Fig. S10 Transient piezoelectric current response of SnS-0.15. Experimental conditions: [Na_2SO_4] = 1 M, applied potential of –0.02 V vs Ag/AgCl, and Pt wire was employed as the counter electrode.

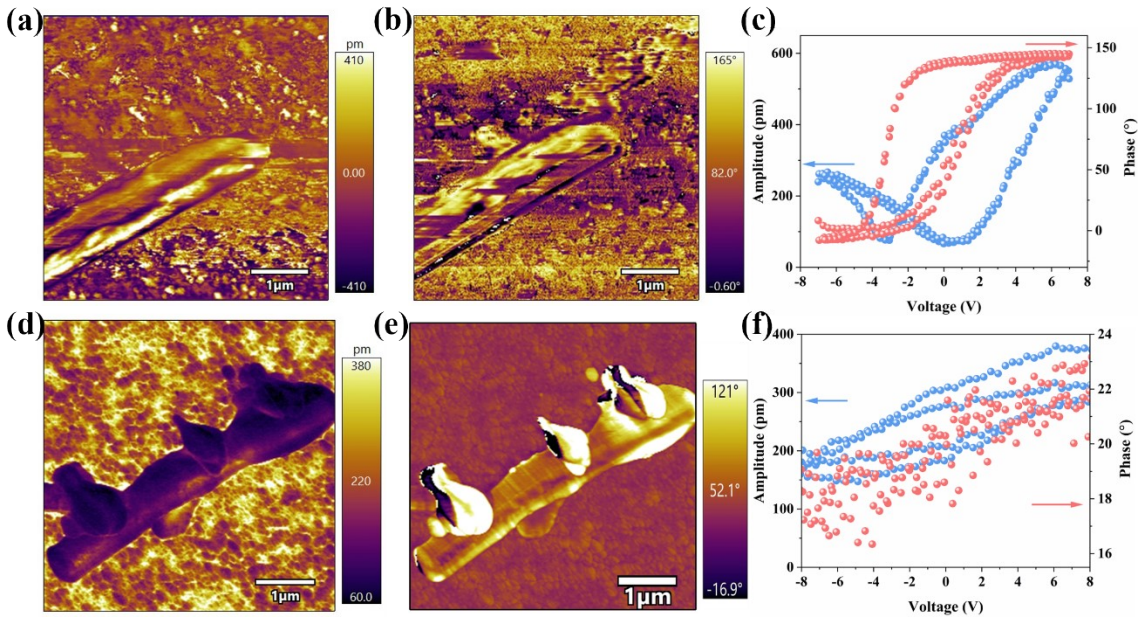

Fig. S11 The amplitude, phase images and amplitude-/phase-voltage curves of (a-c) SnS-0.25, and (d-f) SnS-0.45.

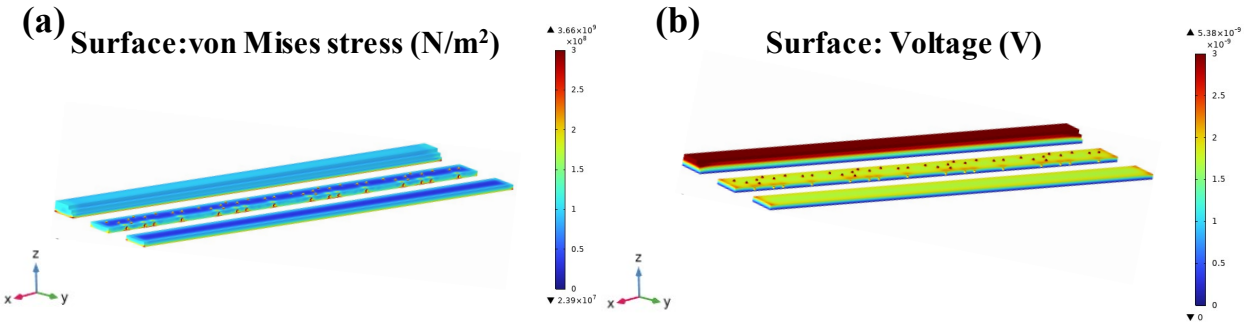

Fig. S12 COMSOL simulations on SnS nanobelts under the stress process. (a) The stress on SnS surface, (b) The piezoelectric potential distribution on SnS surfaces.

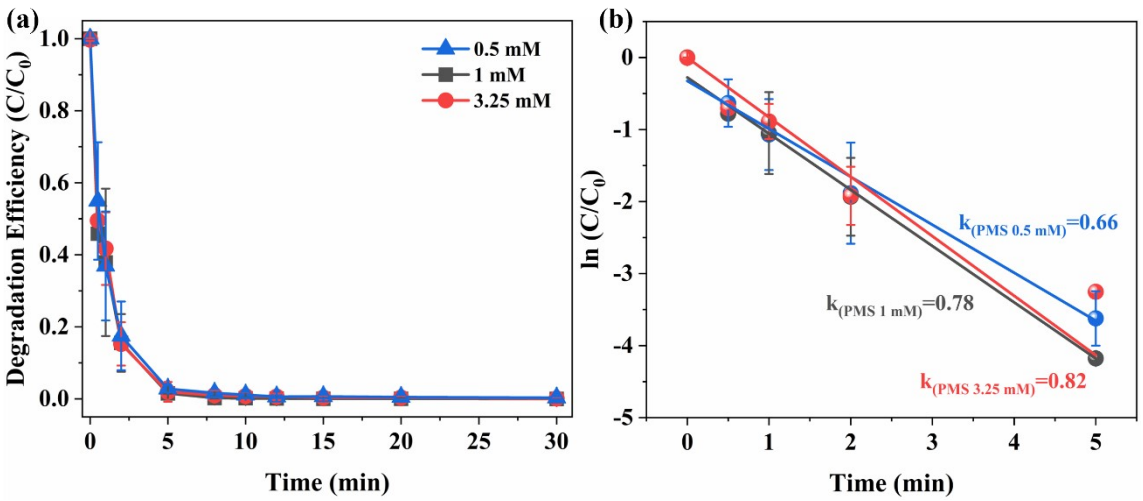

Fig. S13 (a) Effects of PMS concentration on APAP decomposition kinetics in US/PMS/SnS-0.15 system, (b) corresponding kinetic rate fitting. Experimental conditions: [SnS] = 0.4 g L^{-1}, [APAP] = 20 μM, T = 25 °C, vibration source: 40 KHz ultrasound.

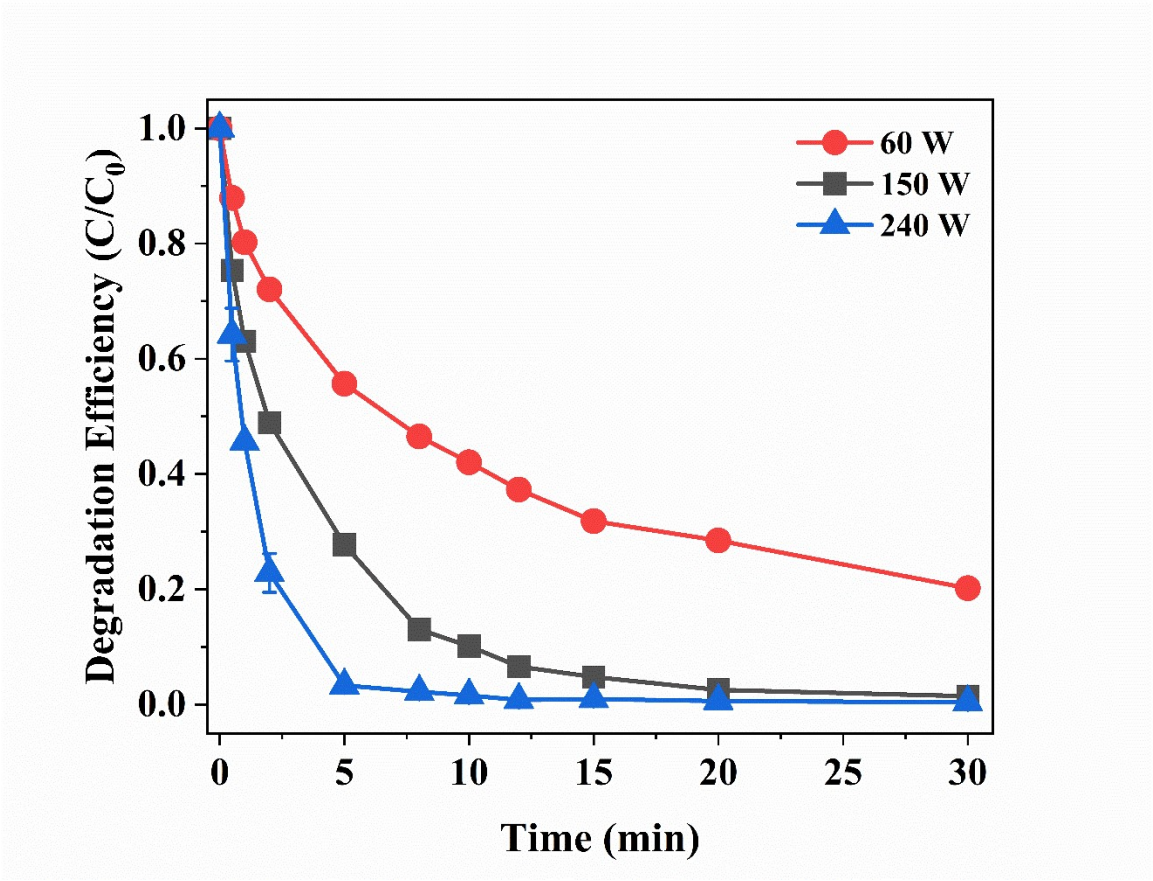

Fig. S14 Effects of US intensity on APAP degradation in US/PMS/SnS-0.15 system. Experimental conditions: [PMS] = 0.5 mM, [SnS] = 0.4 g L^{-1}, [APAP] = 20 μM, T = 25 °C, vibration source: 40 KHz ultrasound.

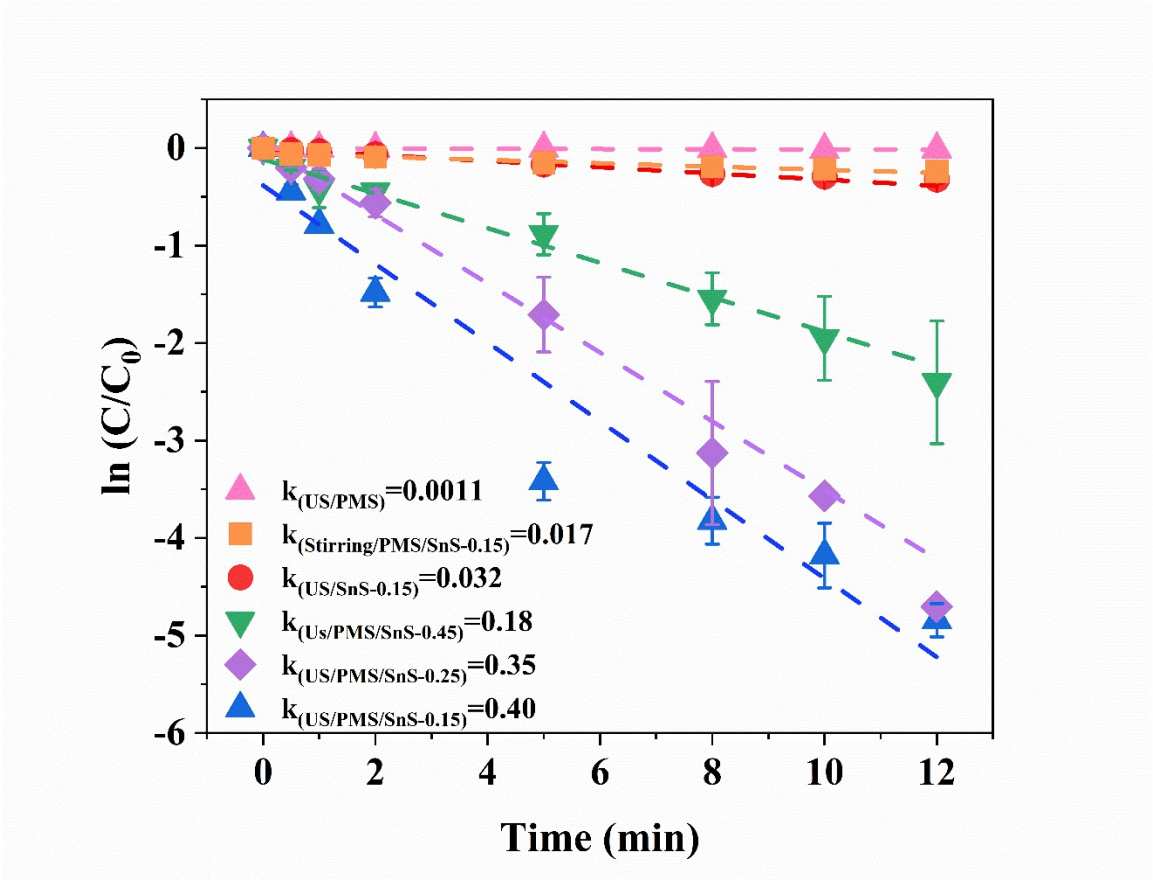

Fig. S15 First-order linear fitting curves in different systems. Experimental conditions: [PMS] = 0.5 mM, [SnS] = 0.4 g L^{-1}, [APAP] = 20 μM, T = 25 °C, vibration source: 40 KHz ultrasound.

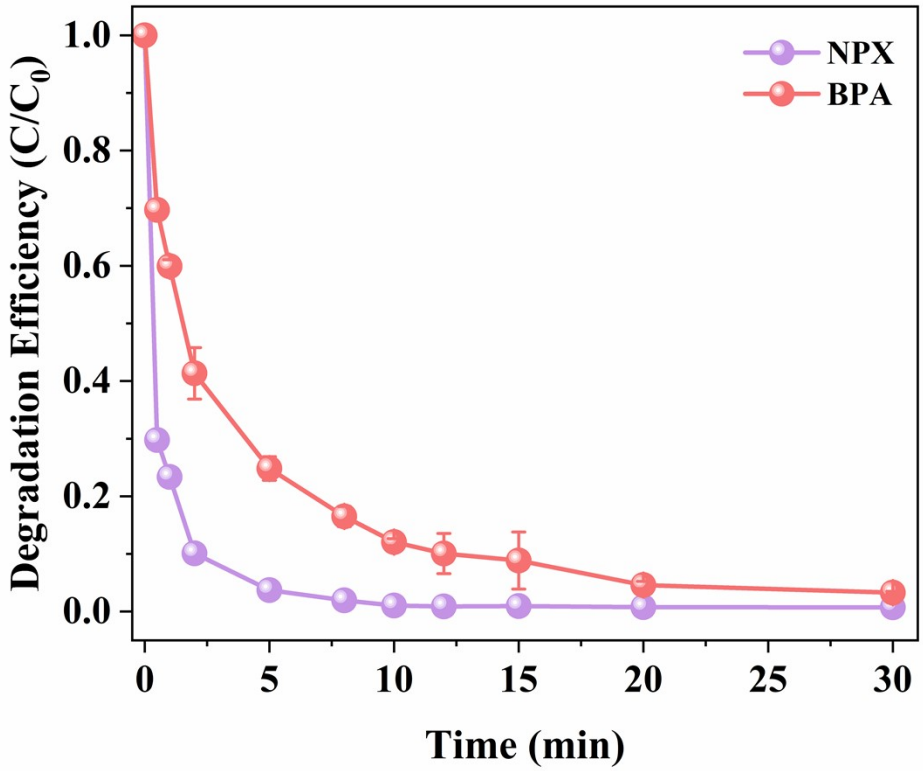

Fig. S16 BPA and NPX degradation kinetics in the US/PMS/SnS-0.15 system. Experimental conditions: [PMS] = 0.5 mM, [SnS] = 0.4 g L^{-1}, [BPA] = [NPX] = 20 μM, T = 25 °C, vibration source: 40 KHz ultrasound.

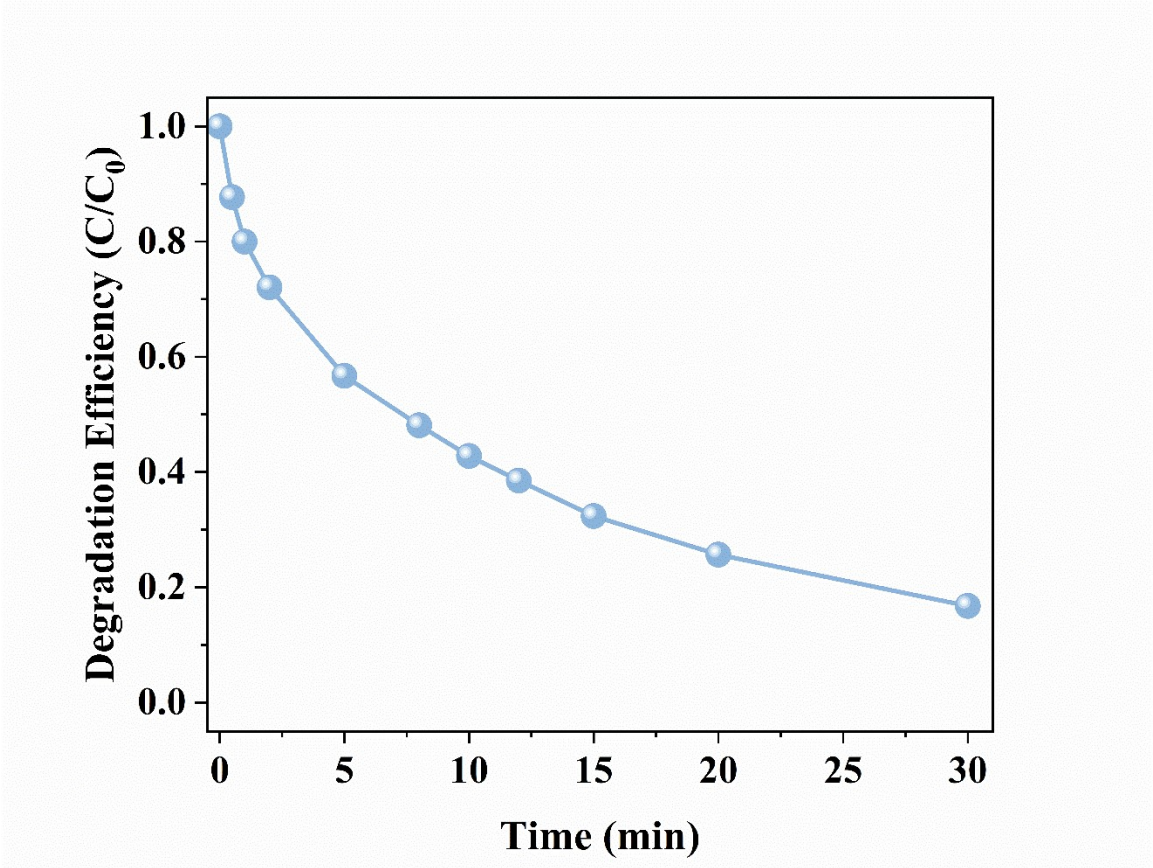

Fig. S17 Degradation kinetics of APAP in the US/PMS/SnS-0.15 with tap water. Experimental conditions: [PMS] = 0.5 mM, [SnS] = 0.4 g L^{-1}, [APAP] = 20 μM, T = 25 °C, vibration source: 40 KHz ultrasound.

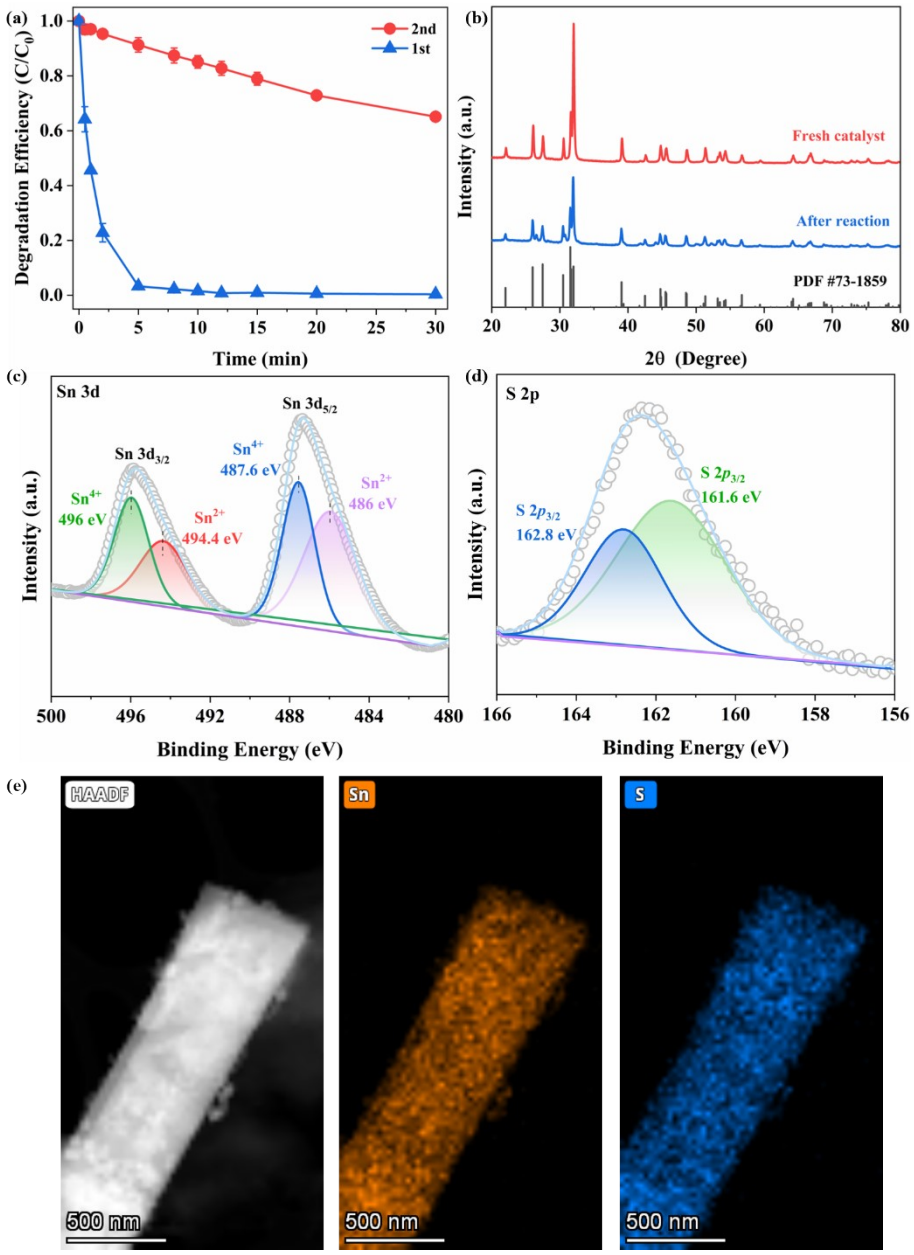

Fig. S18 (a) The recycling experiment in the US/PMS/SnS-0.15. (b) XRD pattern of SnS-0.15 before and after reaction. XPS spectra of SnS-0.15 after reaction: (c) Sn 3d, (d) S 2p. (e) HADDF-STEM and EDS-mapping images of SnS-0.15 after reaction.

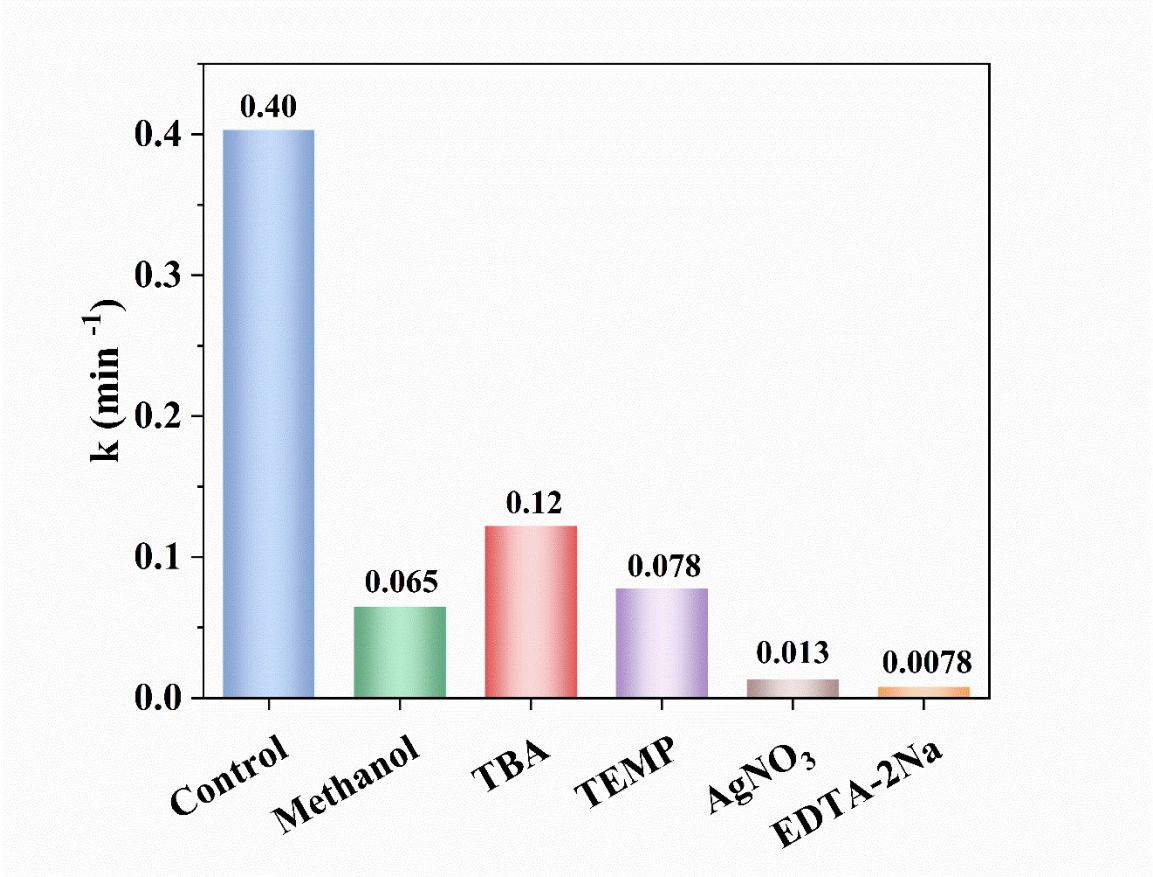

Fig. S19 Corresponding reaction rate constants for APAP degradation using different scavengers in US/PMS/SnS-0.15 system.

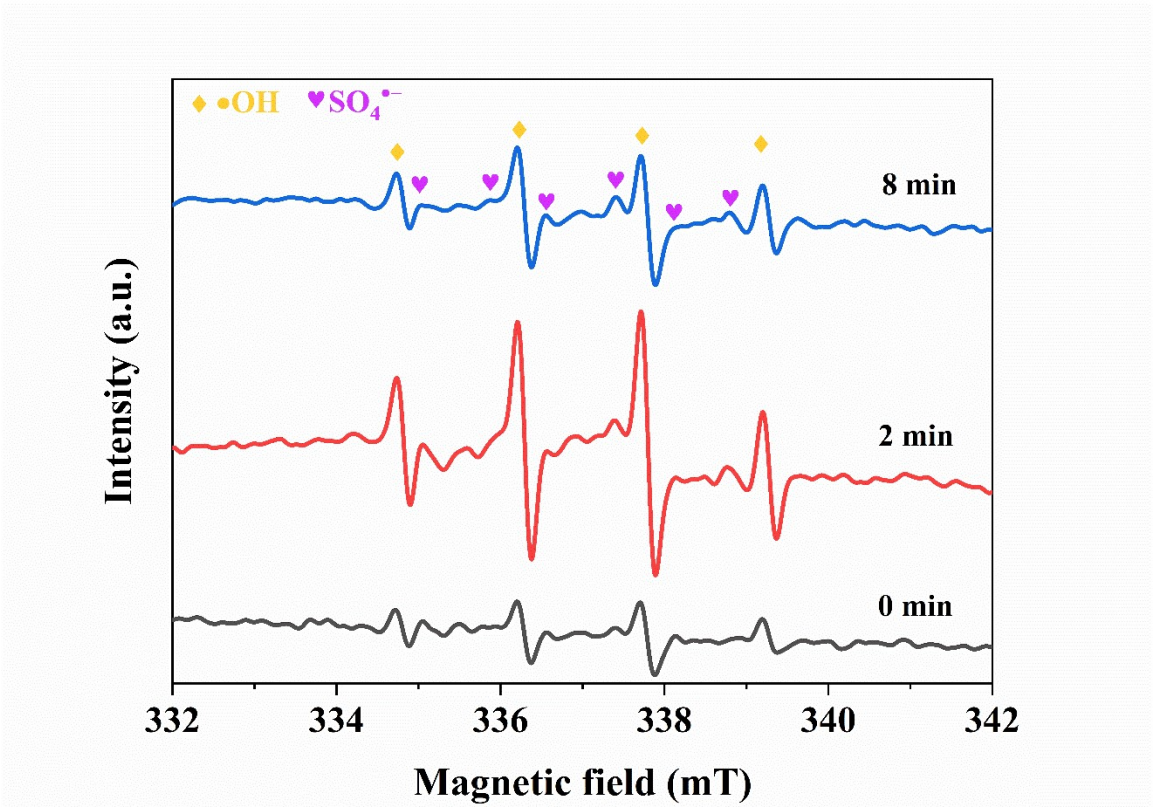

Fig. S20 Variation of EPR signals for •OH and SO_4•$^{-}$ in US/PMS/SnS-0.15 system with time. Experimental conditions: [PMS] = 0.5 mM, [SnS] = 0.4 g L^{-1}, [DMPO] = 50 mM.

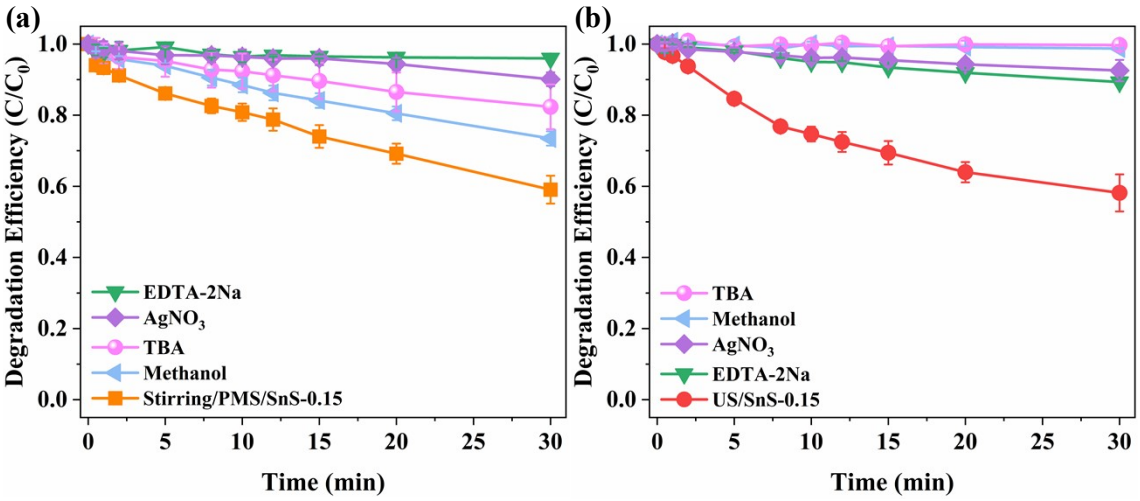

Fig. S21 Quenching experiments for different systems, (a) Stirring/PMS/SnS-0.15, (b) US/SnS-0.15. Experimental conditions: [PMS] = 0.5 mM, [SnS] = 0.4 g L^{-1}, [APAP] = 20 μM, [TBA] = [Methanol] = 200 mM, [EDTA-2Na] = [$AgNO_3$] = 2.5 mM. T = 25 °C, vibration source: 40 KHz ultrasound.

Table S1 Comparison of parameters of PMS activated by different piezoelectric materials in piezo-AOP systems.

Piezocatalyst	Catalysts dosage ($g\ L^{-1}$)	PMS dosage (mM)	Conditions	Performance	Refs
MoS_2	0.5	6	100 W, 40 kHz	99% degradation of phenol in 15 min	[1]
MoS_2 NFs	0.3	3.25	300 W, 40 kHz	95% degradation of phenol in 180 min	[2]
$BaTiO_3$	0.5	3.25	100 W, 40 kHz	97% degradation of BTH within 30 min	[3]
$BaTiO_3$	0.5	20	Hydraulic force, stirring	76.17% removal of CBZ in 180 min	[4]
MoS_2	0.4	32.5	300 W	85.0% degradation rate of 4-CP in 120 min	[5]
CNTs/$BaTiO_3$	5	20	hydraulic-driven	91.93% removal rate of CBZ in 120 min	[6]
MoS_2	0.5	1.625	water vortex-driven, stirring	91.1 % degradation of BTR in 5 min	[7]
ZnO	0.5	1.625	100 W, 40 kHz	~100% IBP removal in 50 min	[8]
MoS_2-embedded polyvinylidene fluoride membrane	-	1.625	240 W, 40 kHz	90% degradation of CBZ in 120 min	[9]
Co_3S_4/MoS_2	0.6	9.75	300 W, 40 kHz	99.9% degradation of phenol and CO production (17.33 μmol g^{-1} h^{-1})	[10]
$BiVO_4$	0.5	0.65	100 W, 40 kHz, 300 W xenon lamp	70% degradation of TC in 60 min	[11]
ZnO	0.3	1.625	100 W, 40 kHz	89.9% degradation of ORZ in 60 min	[12]
C_3N_5	0.5	0.975	Ultrasonicator/300 W Xe lamp	98% degradation of RhB in 15 min	[13]
$BaTiO_3$	1	5	aeration	Achieve ~3.0-log removal of ARGs from water within 1 h.	[14]
α-$SnWO_4$/ZnO	1	1.95	100 W, 40 kHz + 300 W xeon lamp	90.6% degradation of CBZ in 120 min	[15]
MoS_2	0.1	3.25	150 W, 40 kHz	92.1% RhB degradation after 25 min	[16]
Co-$BaTiO_3$	0.2	1.625	200 W, 40 kHz	100% removal of ATZ in 30 min	[17]

References

1. G. Nie, L. Xiao, J. Bi, S. Wang and X. Duan, *Appl. Catal. B Environ.*, 2022, **315**, 121584.
2. S. Liu, B. Jing, C. Nie, Z. Ao, X. Duan, B. Lai, Y. Shao, S. Wang and T. An, *Environ. Sci. Nano*, 2021, **8**, 784-794.
3. S. Lan, Y. Chen, L. Zeng, H. Ji, W. Liu and M. Zhu, *J. Hazard. Mater.*, 2020, **393**, 122448.
4. Y. Zheng, J. Yang, B. Gong, X. Zhang, J. Li, H. Zheng, G. Chen and C. Zhao, *Chem. Eng. J.*, 2022, **441**, 136116.
5. F. Cao, L. Yang, Y. Zhang, X. Zhao, H. Lu and J. Wang, *J Clean. Prod.*, 2022, **380**, 135002.
6. Y. Zheng, W. Zhuang, X. Zhang, J. Xiang, X. Wang, Z. Song, Z. Cao and C. Zhao, *Chem. Eng. J.*, 2022, **449**, 137826.
7. C. Yu, J. He, S. Lan, W. Guo and M. Zhu, *Environ. Sci. Ecotechnology*, 2022, **10**, 100165.
8. M. Zhang, H. Tao, C. Zhai, J. Yang, Y. Zhou, D. Xia, G. Comodi and M. Zhu, *Appl. Catal. B Environ.*, 2023, **326**, 122399.
9. E. Wu, Y. Yu, J. Hu, G. Ren and M. Zhu, *J. Hazard. Mater.*, 2023, **458**, 131885.
10. M. Ran, H. Xu, Y. Bao, Y. Zhang, J. Zhang and M. Xing, *Angew. Chem., Int. Ed.*, 2023, **62**, e202303728.
11. H. Wang, Z. Long, R. Chen, H. Zhang, H. Shi and Y. Chen, *Sep. Purif Technol*, 2024, **331**, 125598.
12. J. Yang, M. Zhang, M. Chen, Y. Zhou and M. Zhu, *Adv. Mater*, 2023, **35**, e2209885.
13. C. Fu, M. Zhao, X. Chen, G. Sun, C. Wang and Q. Song, *Appl. Catal. B Environ.*, 2023, **332**, 122752.
14. J. Li, L. Yu, M. Liu, Y. Xie and Y. Yu, *Environ Pollut*, 2024, **347**, 123687.
15. X. Zhou, Y. Liu, Y. Miao, W. He, Y. Pan, A. Jing Li, J. Qin, H. Li, R. Yin and R. Qiu, *Sep. Purif. Technol.*, 2023, **323**, 124410.
16. S. Li, X. Ning, P. Hao, Y. Cao, J. Xie, J. Hu, Z. Lu and A. Hao, *Dyes and Pigments*, 2022, **206**, 124410.
17. S. Xiong, H. Zeng, R. Tang, L. Li, Z. Zhou, J. Wang, C. Ding, D. Gong and Y. Deng, *Chem. Eng. J.*, 2023, **466**, 143200.